# Electronic phase diagram of epitaxial $La_{1-x}Sr_xFeO_3$ films

Y. J. Xie, M. D. Scafetta, E. J. Moon, A. L. Krick, R. J. Sichel-Tissot, and S. J. May[a)]
*Department of Materials Science and Engineering, Drexel University, Philadelphia, Pennsylvania 19104, USA*

(Received 22 July 2014; accepted 1 August 2014; published online 14 August 2014)

The electronic phase diagram of epitaxial $La_{1-x}Sr_xFeO_3$ films is presented. The films were grown on $SrTiO_3$ using molecular beam epitaxy with post-growth annealing to minimize oxygen vacancies. Insulating behavior is observed from $x = 0$–0.9, with metallic conduction only present for $x = 1.0$. While the La-rich compounds exhibit polaron conduction over all temperatures measured, the Sr-rich films exhibit an electronic phase transition within the compositional window of $x = 0.49$–0.9 as revealed by temperature-dependent resistivity measurements. The transition temperatures are found to decrease with increasing Sr content. The constructed phase diagram is discussed in the context of other $3d$ $e_g$ perovskite systems including manganites and cobaltites.  [http://dx.doi.org/10.1063/1.4893139]

The $3d$ perovskite oxides of the chemical form $ABO_3$, where $A$ and $B$ are cations, exhibit a host of interesting physical phenomena.[1] In many cases, the electronic or magnetic ground state can be tuned between energetically similar phases through slight modifications to the nominal valence state of the $B$-site cation or the topology of the corner-connected $BO_6$ octahedra. The most common route to induce these modifications is through alloying multiple cations on the $A$-site. Phase diagrams generated by studies of $A_xA'_{1-x}BO_3$ solid solutions have been critical in better understanding the exceedingly rich physics of titanates,[2,3] manganites,[4–7] and cobaltites.[8] The $La_{1-x}Sr_xFeO_3$ (LSFO) system is also known to exhibit interesting phenomena including nominally charge disproportionated states[9–11] and exotic magnetic structures.[12–15] However, compared to its manganite and cobaltite counterparts, less is known regarding the evolution of electronic behavior across the entire phase diagram from $x = 0$–1. Furthermore, the evolution of transport properties as a function of composition in strained $La_{1-x}Sr_xFeO_3$ thin films remains relatively unexplored.

The parent compound $LaFeO_3$ is an insulator with a $3d^5$ Fe electronic configuration. The filled majority $t_{2g}$ and $e_g$ orbitals give rise to G-type antiferromagnetism with a Neel temperature ($T_N$) of 750 K.[16] Substitution of Sr on the $A$-site adds a hole to the hybridized $3d$ Fe-$2p$ O states,[17–19] resulting in increased electrical conductivity and a decreased $T_N$.[10,20] Detailed structural studies of bulk LSFO revealed alloying-induced structural transitions from orthorhombic $Pbnm$ to rhombohedral $R\bar{3}c$ at $x \sim 0.25$ and $R\bar{3}c$ to cubic $Pm3m$ at $x \sim 0.75$.[21,22] The $La_{1/3}Sr_{2/3}FeO_3$ composition exhibits a simultaneous charge disproportionation (CD) and magnetic ordering transition near 190 K, in which the nominal CD periodicity is $3d_{111}$ and the spin structure periodicity is $6d_{111}$.[23] The other parent compound, $SrFeO_3$, is metallic with helimagnetic order along the [111].[14] Electronically, previous work has established that three behaviors are present in LSFO: an insulating phase in La-rich compounds, the CD phase when Sr-rich, and the metallic phase in $SrFeO_3$. However, the compositional boundaries between these phases remain unclear and a complete phase diagram of electronic behavior as a function of composition and temperature from consistently synthesized materials has yet to be presented.

In this work, we establish a complete electronic phase diagram from $x = 0$–1 for epitaxial LSFO films on $SrTiO_3$ (STO) substrates. We find the nominally CD phase exists in a half-dome from $x \sim 0.49$–0.9, with the transition temperature decreasing as the Sr content is increased. We also identify polaron conduction as the dominant transport mechanism throughout the non-charge disproportionated insulating regions of the phase diagram.

The LSFO films were deposited by oxide molecular beam epitaxy in pressures of 2–8 $\times$ $10^{-6}$ Torr achieved by the introduction of a dilute ozone in oxygen mixture to the growth chamber.[24] Co-deposition of the cations was followed by short pauses, yielding a growth rate of ~40–60 s per unit cell. Growth temperatures ranged from 550 to 650 °C. Following deposition, the films were annealed at 675 °C in $O_2$ for 2–4 h, cooled to 200 °C and exposed to a $O_3/O_2$ mixture (~5:95) for 30–60 min to minimize oxygen vacancies.[25,26] All data reported herein were obtained from films following the post-growth annealing process. The cation compositions of the films used in this study were measured by Rutherford backscattering spectroscopy (RBS) with the SIMNRA software used to simulate spectra. The difference squared between the measured and calculated spectra was minimized as a function of each cation composition to determine the film stoichiometry.[27] Representative RBS spectra and simulations are shown in Fig. 1(a). The film thicknesses ranged from 60 to 135 unit cells. A table of the exact compositions and thicknesses can be found in the supplementary material.[28]

X-ray diffraction was used to measure c-axis parameters and confirm sample quality. Diffraction patterns of representative samples are illustrated in the inset of Fig. 1(b). The replacement of La by Sr induces a shift of the (002) film peak indicative of a decreased lattice parameter, consistent with bulk LSFO.[21,29] The c-axis parameters were quantified by simulating the film and substrate (002) peaks using the GenX software package.[30] The obtained lattice parameters

[a)]Electronic mail: smay@coe.drexel.edu

 

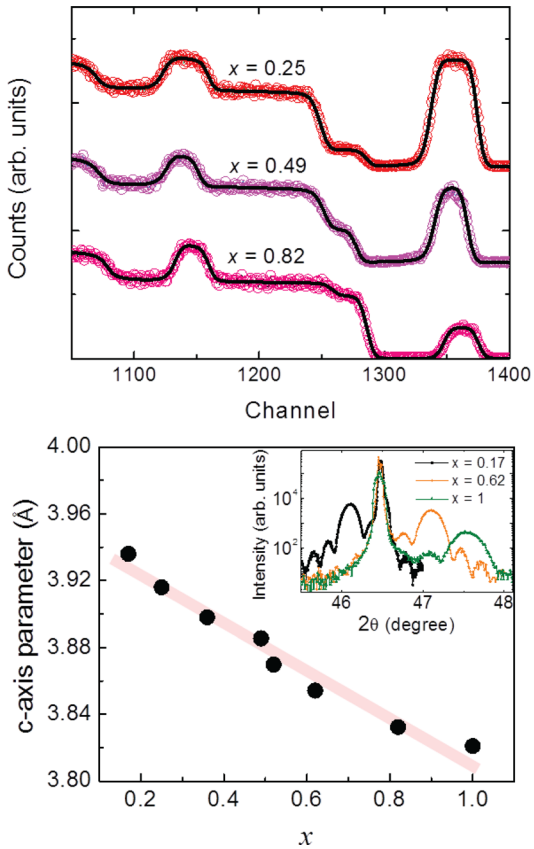


FIG. 1. Representative RBS data and simulations (a) from three LSFO films on $SrTiO_3$. The c-axis parameter as a function of Sr composition, as determined from the x-ray diffraction data, is shown in (b). Representative (002) diffraction peaks are shown in the inset of (b). The differences in peak intensity and width arise from differences in film thickness. For example, the $x = 0.17$ film is 52 nm, while the $x = 1$ film is 32 nm.

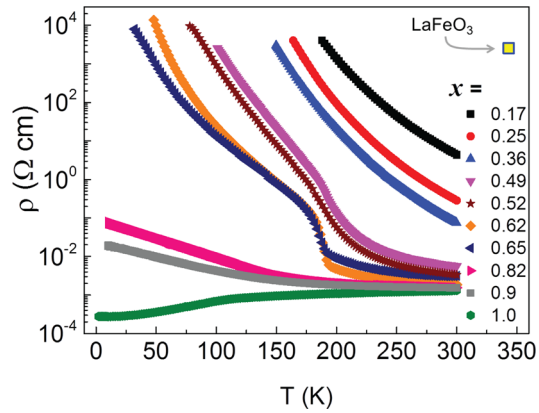


FIG. 2. Temperature dependent resistivity for the LSFO films. The resistivity of a $LaFeO_3$ film is represented by the single square at 340 K.

across the phase diagram are shown in Fig. 1(b), revealing a systematic decrease with increasing Sr content. The lattice reduction is attributed to the smaller atomic radii of the nominal $Fe^{4+}$ cation compared to the $Fe^{3+}$ resulting from the substitution of Sr. In bulk LSFO, a psuedocubic lattice parameter of 3.905 Å, the same lattice parameter as $SrTiO_3$, is found at $x = 0.3$.[29] Therefore, the films with $x \leq 0.25$ are under compressive strain, while those with $x \geq 0.36$ are under tensile strain, consistent with the measured c-axis parameters of the films. The magnitude of the strain varies from 0.7% compressive strain for $LaFeO_3$ to 1.4% tensile strain for $SrFeO_3$.

In-plane DC resistivity was measured as a function of temperature using a four point probe geometry with silver paint used to make contacts. The transport measurements were carried out in a Physical Properties Measurement System (Quantum Design) with an external current source and nanovoltmeter. The results are shown in Fig. 2. Three distinct compositions regimes are apparent. In the La-rich films ($x \leq 0.36$), insulating behavior is observed with the resistivity increasing orders of magnitude as the films are cooled. For these samples, the room temperature resistivity increases by orders of magnitude as the Sr content is decreased. Measurements of $LaFeO_3$ were not possible at room temperature as the films are too insulating, with $\rho$ greater than $10^4$ Ω cm at 300 K; instead, the resistivity of $LaFeO_3$ at 340 K is shown in Fig. 2 for comparison to Sr-containing films.

The second compositional regime exists between $0.49 \leq x \leq 0.9$, where an abrupt increase in the resistivity is observed upon cooling. This non-monotonic resistivity behavior, indicative of an electronic phase transition, is attributed to the formation of a nominally CD and spin ordered state at low temperatures, which localizes carriers.[23] The presence of this ordered state has been studied extensively in $La_{1/3}Sr_{2/3}FeO_3$, in which Mossbauer spectroscopy, electron diffraction, and synchrotron scattering have been used to establish an ordering of hybridized Fe-O states along the [111] direction.[9,31,32] We have previously confirmed the presence of CD in thin $x = 0.67$ films grown under similar conditions on $SrTiO_3$ using synchrotron diffraction,[33] supporting our assignment of the CD phase in the presently studied films. This CD phase has also been previously reported in $x = 0.67$ films grown by pulsed laser deposition.[13,34,35] We note two other interesting features of this compositional range. First, the room temperature resistivity is far less sensitive to Sr content compared to the La-rich films. On the Sr-rich side of the phase, the room temperature resistivity ranges from roughly $10^{-3}$–$10^{-2}$ Ω cm with the resistivity decreasing slightly with increasing Sr content. Second, the CD transition is not a conventional metal-insulator transition in that the resistivity increases with decreasing temperature on both sides of the transition.

The third distinct class of behavior is exhibited by $SrFeO_3$, which is metallic as evidenced by the decreasing resistivity with decreasing temperature. A central challenge with obtaining high quality $SrFeO_3$ films is to avoid large quantities of oxygen vacancies which give raise to a variety of stable $SrFeO_{3-\delta}$ phases.[36] The magnitude of the low temperature resistivity and the presence of a kink in the resistivity around 110 K is consistent with bulk $SrFeO_3$,[12,14] in agreement with previous results that the post-growth anneals in dilute ozone can yield nominally oxygen stoichiometric films[25,37] even under 1.4% tensile strain as is the case with $SrFeO_3$ on $SrTiO_3$.[38]

We next turn to the nature of the insulating state in the La-rich compositions and in the high temperature phase (charge disordered) of the Sr-rich compositions. The temperature dependent resistivity data within these regions is well

described by $\rho = \rho_0 T^{3/2} e^{E_A/kT}$ indicative of non-adiabatic polaron conduction, as shown in the inset of Fig. 3. The observation of polaronic conduction is consistent with previous reports of electronic transport in perovskite ferrites.[39–41] The obtained activation energies ($E_A$) provide another distinction between the La-rich and Sr-rich phases, with a step-like decrease in $E_A$ observed at half-doping. As presented in Fig. 3, the $E_A$ values are between 0.3 and 0.35 eV for $x < 0.45$ and less than 0.15 eV for $x > 0.45$.

Based on the resistivity data obtained from these 10 samples, we are able to construct an electronic phase diagram providing insights into the phase boundaries between the polaronic insulating, CD, and metallic phases. The phase diagram is shown in Fig. 4. At half-doping, a half-dome of the CD phase is present (green in Fig. 4), with the transition temperature (T*) decreasing with increasing Sr content. Our delineation between the CD phase and the metallic phase (red in Fig. 4) is approximate, as we have not investigated samples with $0.91 < x < 0.99$. We place the boundary of the purely insulating and CD phases between $x = 0.4$ and 0.49, as a previous study of an $x = 0.4$ film on STO did not report an inflection in the resistivity.[19]

The obtained ferrite phase diagram provides an interesting contrast to that of $La_{1-x}Sr_xMnO_3$ and $La_{1-x}Sr_xCoO_3$, the two other perovskite families similar to LSFO due to the prominent role played by $3d$ $e_g$ carriers in their physical properties. Both the manganites and cobaltites exhibit a transition from insulating to metallic behavior between $x = 0.15$–$0.18$.[8,42] In contrast, the ferrites remain insulating across the phase diagram despite carrier concentrations well in excess of those needed to trigger metallic behavior in manganites and cobaltites. What can account for this difference? While the polaronic nature of conduction in ferrites undoubtedly contributes to their insulating behavior, polarons have also been reported in manganites.[43] Instead, we hypothesize that the difference in the nominal $B$-site $e_g$ electronic configuration and the resultant magnetic interactions play a key role. The manganites move from a nominal $e_g^1$ to $e_g^0$ configuration as Sr is substituted for La. In these systems, the metallic phase is also ferromagnetic, which is stabilized due to double exchange arising from full-empty $e_g$

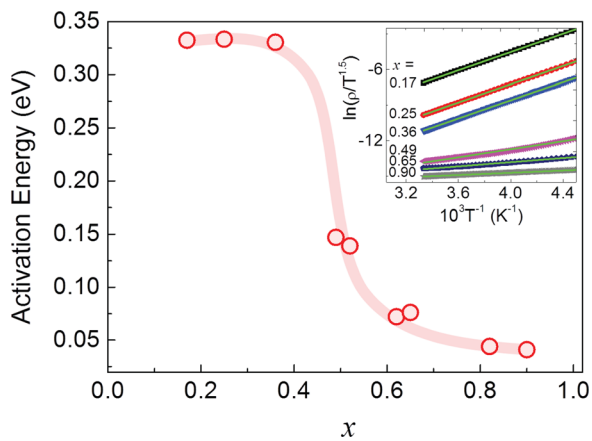


FIG. 3. The obtained activation energies associated with polaron conduction are shown as a function of Sr content. The activation energy abruptly decreases near half-doping. Fits of resistivity data to the polaron conduction model are shown in the inset.

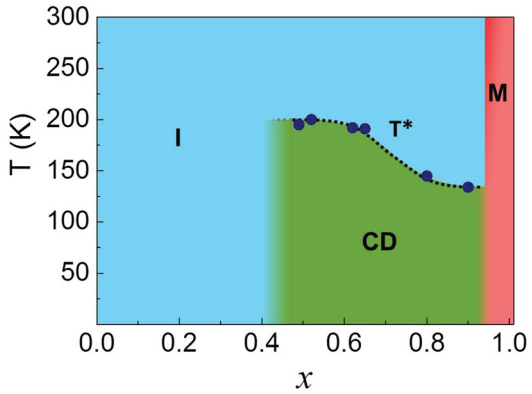


FIG. 4. The electronic phase diagram of LSFO. The blue regions correspond to insulating, polaronic conduction; the green region corresponds to the nominally CD phase; the red region corresponds to the metallic phase. The smeared out regions between $x = 0.4$–$0.49$ and 0.9–1 represent in the uncertainty in the phase boundaries.

interactions. In LSFO, the substitution of Sr for La alters the nominal electronic configuration from $e_g^2$ to $e_g^2$ plus a hole in a hybridized O-Fe state.[17,44–46] In this case, any ferromagnetic interactions compete with antiferromagnetic full-full $e_g$ and $t_{2g}$ interactions. The multiple antiferromagnetic exchange interactions are energetically favorable, stabilizing G-type antiferromagnetic order from $x = 0 \leq 0.4$.[16,47] We assert that the antiferromagnetic state is critical in promoting the insulating ground state. At doping levels greater than $x = 0.5$, magnetic exchange is also believed to be a critical component in stabilizing the CD phase in LSFO,[11] which results in insulating behavior.

Finally, we comment on how the properties observed in the films compare to previous reports of bulk LSFO. We find the general trends in resistivity and T* to be in agreement with reports from bulk LSFO, suggesting that the strain induced by the STO substrate is not fundamentally altering the electronic ground at the compositions studied here. The measurements performed by Maeder and Bednorz on LSFO single crystals provide a systematic sample set for comparison.[20] The bulk crystals with $x = 0.2$, 0.3, and 0.4 are insulating without evidence of CD transitions, while a bulk $x = 0.5$ sample exhibits a slight kink in resistivity near 200 K, consistent with our observations from films. On the side of the phase diagram containing the CD phase, our data are in agreement with polycrystalline bulk samples studied by Matsuno *et al.*,[10] who find a decrease in T* from approximately 200 to 150 K and a less abrupt change in resistivity as $x$ is increased from 0.67 to 0.8. Similarly, Blasco and coauthors report a T* of approximately 190 and 160 K for $x = 0.67$ and 0.75, respectively.[48] However, these results stand in contrast to a $x = 0.8$ single crystal, in which Maeder and Bednorz observed a transition temperature of 205 K, considerably higher than in our $x = 0.82$ film. Given that T* of the bulk crystal does not exhibit a strong dependence on oxygen content, T* = 205 and 200 K for $La_{0.2}Sr_{0.8}FeO_{2.99}$ and $La_{0.2}Sr_{0.8}FeO_{2.91}$,[20] we attribute the suppressed transition temperature in the films compared to the single crystals to either the biaxial tensile strain induced by the STO substrate or error in the cation concentration, as we find T* to be sensitive to $x$.

In conclusion, we have presented a complete electronic phase diagram spanning $x = 0$–1 for epitaxial $La_{1-x}Sr_xFeO_3$

thin films on $SrTiO_3$. We find insulating behavior on the La-rich side of the diagram, an electronic phase transition present between $x = 0.49$–$0.9$, and metallic behavior in $SrFeO_3$. These results help to establish the general electronic behavior of this perovskite family as well as point to compositional ranges that warrant future study, such as the phase boundary separating the CD and metallic phases between $x = 0.9$–$1$.

We thank Boris Yakshinskiy for RBS measurements at the Rutgers University Laboratory for Surface Modification. This work was supported by the Office of Naval Research under Grant Nos. N00014-11-1-0109 (synthesis of $x < 0.4$ films) and N00014-11-1-0664. M.D.S. acknowledges support from the Department of Education (GAANN-RETAIN, Award No. P200A100117). Acquisition of the Physical Properties Measurement System was supported by the U.S. Army Research Office under Grant No. W911NF-11-1-0283. The x-ray diffractometer was acquired with funds from NSF MRI Award DMR-1040166.

[1]J. B. Goodenough, Rep. Prog. Phys. **67**, 1915 (2004).
[2]Y. Tokura, Y. Taguchi, Y. Okada, Y. Fujishima, T. Arima, K. Kumagai, and Y. Iye, Phys. Rev. Lett. **70**, 2126 (1993).
[3]C. C. Hays, J.-S. Zhou, J. T. Markert, and J. B. Goodenough, Phys. Rev. B **60**, 10367 (1999).
[4]P. Schiffer, A. P. Ramirez, W. Bao, and S.-W. Cheong, Phys. Rev. Lett. **75**, 3336 (1995).
[5]C. Martin, A. Maignan, M. Hervieu, and B. Raveau, Phys. Rev. B **60**, 12191 (1999).
[6]O. Chmaissem, B. Dabrowski, S. Kolesnik, J. Mais, J. D. Jorgensen, and S. Short, Phys. Rev. B **67**, 094431 (2003).
[7]I. Kézsmárki, Y. Tomioka, S. Miyasaki, L. Demkó, Y. Okimoto, and Y. Tokura, Phys. Rev. B **77**, 075117 (2008).
[8]C. He, M. A. Torija, J. Wu, J. W. Lynn, H. Zheng, J. F. Mitchell, and C. Leighton, Phys. Rev. B **76**, 014401 (2007).
[9]P. D. Battle, T. C. Gibb, and P. Lightfoot, J. Solid State Chem. **84**, 271 (1990).
[10]J. Matsuno, T. Mizokawa, A. Fujimori, K. Mamiya, Y. Takeda, S. Kawasaki, and M. Takano, Phys. Rev. B **60**, 4605 (1999).
[11]R. J. McQueeney, J. Ma, S. Chang, J.-Q. Yan, M. Hehlen, and F. Trouw, Phys. Rev. Lett. **98**, 126402 (2007).
[12]P. Adler, A. Lebon, V. Damljanovic, C. Ulrich, C. Bernhard, A. V. Boris, A. Maljuk, C. T. Lin, and B. Keimer, Phys. Rev. B **73**, 094451 (2006).
[13]J. Okamoto, D. J. Huang, K. S. Chao, S. W. Huang, C.-H. Hsu, A. Fujimori, A. Masuno, T. Terashima, M. Takano, and C. T. Chen, Phys. Rev. B **82**, 132402 (2010).
[14]S. Ishiwata, M. Tokunaga, Y. Kaneko, D. Okuyama, Y. Tokunaga, S. Wakimoto, K. Kakurai, T. Arima, Y. Taguchi, and Y. Tokura, Phys. Rev. B **84**, 054427 (2011).
[15]M. Reehuis, C. Ulrich, A. Maljuk, Ch. Niedermayer, B. Ouladdiaf, A. Hoser, T. Hofmann, and B. Keimer, Phys. Rev. B **85**, 184109 (2012).
[16]W. C. Koehler and E. O. Wollan, J. Phys. Chem. Solids **2**, 100 (1957).
[17]M. Abbate, F. M. F. de Groot, J. C. Fuggle, A. Fujimori, O. Strebel, F. Lopez, M. Domke, G. Kaindl, G. A. Sawatzky, M. Takano, Y. Takeda, H. Eisaki, and S. Uchida, Phys. Rev. B **46**, 4511 (1992).
[18]A. Chainani, M. Mathew, and D. D. Sarma, Phys. Rev. B **48**, 14818 (1993).
[19]H. Wadati, D. Kobayashi, H. Kumigashira, K. Okazaki, T. Mizokawa, A. Fujimori, K. Horiba, M. Oshima, N. Hamada, M. Lippmaa, M. Kawasaki, and H. Koinuma, Phys. Rev. B **71**, 035108 (2005).
[20]T. Maeder and J. G. Bednorz, J. Eur. Ceram. Soc. **19**, 1507 (1999).
[21]S. E. Dann, D. B. Currie, M. T. Weller, M. F. Thomas, and A. D. Al-Rawwas, J. Solid State Chem. **109**, 134 (1994).
[22]A. Fossdal, M. Menon, I. Waernhus, K. Wiik, M.-A. Einarsrud, and T. Grande, J. Am. Ceram. Soc. **87**, 1952 (2004).
[23]S. K. Park, T. Ishikawa, Y. Tokura, J. Q. Li, and Y. Matsui, Phys. Rev. B **60**, 10788 (1999).
[24]M. D. Scafetta, Y. J. Xie, M. Torres, J. E. Spanier, and S. J. May, Appl. Phys. Lett. **102**, 081904 (2013).
[25]H. Yamada, M. Kawasaki, and Y. Tokura, Appl. Phys. Lett. **80**, 622 (2002).
[26]Y. Xie, M. D. Scafetta, R. J. Sichel-Tissot, E. J. Moon, R. C. Devlin, H. Wu, A. L. Krick, and S. J. May, Adv. Mater. **26**, 1434 (2014).
[27]L. Qiao, T. C. Droubay, M. E. Bowden, V. Shutthanandan, T. C. Kaspar, and S. A. Chambers, Appl. Phys. Lett. **99**, 061904 (2011).
[28]See supplementary material at http://dx.doi.org/10.1063/1.4893139 for additional information regarding film thicknesses and compositions.
[29]O. Clemens, M. Kuhn, and R. Haberkorn, J. Solid State Chem. **184**, 2870 (2011).
[30]M. Bjorck and G. Andersson, J. Appl. Crystallogr. **40**, 1174 (2007).
[31]M. Takano, J. Kawachi, N. Nakanishi, and Y. Takeda, J. Solid State Chem. **39**, 75 (1981).
[32]J. Herrero-Martin, G. Subías, J. Garcia, J. Blasco, and M. Concepcion Sanchez, Phys. Rev. B **79**, 045121 (2009).
[33]R. J. Sichel-Tissot, R. C. Devlin, J.-W. Kim, P. J. Ryan, and S. J. May, Appl. Phys. Lett. **103**, 212905 (2013).
[34]W. Prellier and B. Mercey, J. Phys. D: Appl. Phys. **35**, L48 (2002).
[35]K. Ueno, A. Ohtomo, F. Sato, and M. Kawasaki, Phys. Rev. B **73**, 165103 (2006).
[36]J. P. Hodges, S. Short, J. D. Jorgensen, X. Xiong, B. Dabrowski, S. M. Mini, and C. W. Kimball, J. Solid State Chem. **151**, 190 (2000).
[37]S. Chakraverty, T. Matsuda, H. Wadati, J. Okamoto, Y. Yamasaki, H. Nakao, Y. Murakami, S. Ishiwata, M. Kawasaki, Y. Taguchi, Y. Tokura, and H. Y. Hwang, Phys. Rev. B **88**, 220405(R) (2013).
[38]E. J. Moon, Y. Xie, E. D. Laird, D. J. Keavney, C. Y. Li, and S. J. May, J. Am. Chem. Soc. **136**, 2224 (2014).
[39]W. H. Jung and E. Iguchi, J. Phys.: Condens. Matter **7**, 1215 (1995).
[40]E. V. Tsipis, M. V. Patrakeev, V. V. Kharton, A. A. Yaremchenko, G. C. Mather, A. L. Shaula, I. A. Leonidov, V. L. Kozhevnikov, and J. R. Frade, Solid State Sci. **7**, 355 (2005).
[41]R. C. Devlin, A. L. Krick, R. J. Sichel-Tissot, Y. J. Xie, and S. J. May, J. Appl. Phys. **115**, 233704 (2014).
[42]A. Seeger, P. Lunkenheimer, J. Hemberger, A. A. Mukhin, V. Y. Ivanov, A. M. Balbashov, and A. Loidl, J. Phys.: Condens. Matter **11**, 3273 (1999).
[43]M. Ziese and C. Srinitiwarawong, Phys. Rev. B **58**, 11519 (1998).
[44]A. E. Bocquet, A. Fujimori, T. Mizokawa, T. Saitoh, H. Namatame, S. Suga, N. Kimizuka, Y. Takeda, and M. Takano, Phys. Rev. B **45**, 1561 (1992).
[45]I. R. Shein, K. I. Shein, V. L. Kozhevnikov, and A. L. Ivanovskii, Phys. Solid State **47**, 2082 (2005).
[46]A. Cammarata and J. M. Rondinelli, Phys. Rev. B **86**, 195144 (2012).
[47]V. G. Sathe, S. K. Paranjpe, V. Siruguri, and A. V. Pimpale, J. Phys.: Condens. Matter **10**, 4045 (1998).
[48]J. Blasco, B. Aznar, J. García, G. Subías, J. Herrero-Martín, and J. Stankiewicz, Phys. Rev. B **77**, 054107 (2008).